Third-order momentum correlation interferometry maps for entangled quantal states of three singly trapped massive ultracold fermions

Constantine Yannouleas [*] and Uzi Landman [†]
School of Physics, Georgia Institute of Technology, Atlanta, Georgia 30332-0430, USA

(Received 23 February 2019; revised manuscript received 7 June 2019; published 22 August 2019)

Analytic higher-order momentum correlation functions associated with the time-of-flight spectroscopy of three ultracold fermionic atoms singly confined in a linear three-well optical trap are presented, corresponding to the W- and Greenberger-Horne-Zeilinger–type states that belong to characteristic classes of tripartite entanglement and represent the strong-interaction regime captured by a three-site Heisenberg Hamiltonian. The methodology introduced here contrasts with and goes beyond that based on the standard Wick factorization scheme; it enables determination of both third-order and second-order spin resolved and spin unresolved momentum correlations, aiming at matter-wave interference investigations with trapped massive particles in analogy with, and having the potential for expanding the scope of, recent three-photon quantum-optics interferometry.

DOI: 10.1103/PhysRevA.100.023618

I. INTRODUCTION

Matter-wave simulations, with highly controlled ultracold atoms, of well-known photon physics have been pursued along two quantum-optics central themes: (i) the coherence properties [1,2] of thermal or chaotic light (in contrast to laser light), studied via second- and higher-order correlations (including the Hanbury Brown–Twiss effect [3]), and (ii) two-photon (or biphoton) interference effects [4–6] associated with fully quantal and entangled photon states (including the Hong-Ou-Mandel effect [7]).

Knowledge of high-order correlations of a quantum many-body system has been long recognized to fully characterize the system under study [1,8–11]. Most recently progress has been demonstrated [12–15] in the development of the theoretical framework for matter-wave interferometry through the use of second-order momentum correlations, measurable in time-of-flight (TOF) laboratory experiments [16,17] (see '*Note added*' at the conclusion of this paper), yielding exact closed-form results based on first-principles (configuration interaction [12,13]) and model Hamiltonian (Hubbard [14,15]) methods.

Here we formulate and implement an accurate and practical methodology for determining higher-order momentum correlation functions for strongly interacting and entangled many-particle systems (beyond the bosonic or fermionic quantum-statistics entanglement contributions), expanding and generalizing the above-mentioned work [12–15]. In particular, our present methodology and derivation of higher-order momentum correlations (here, spin *resolved* and spin *unresolved* third-order correlations), based on the Heisenberg Hamiltonian for three singly trapped ultracold atoms, differ from those relying on the standard Wick factorization scheme [18]. The latter scheme is central to investigations of many-particle correlations in varied fields (including nuclei, condensed matter, atoms and molecules [17], and optics), allowing, *in the absence of interactions*, full factorization (with the use of the Wick method [18,19]) of the N-particle correlation function (the Green's function in the original formulation [18]), $\mathcal{G}^N$ with $N > 2$, as a sum of terms containing antisymmetrized or symmetrized (corresponding to fermions or bosons) products of only $\mathcal{G}^N$'s with $N \leqslant 2$.

Wick's factorization has been employed for Gaussian-type, or single-determinantal, ground states of ultracold atomic clouds [17,20–24], mimicking the methodology, introduced earlier [1,2] for addressing coherence properties of thermal or chaotic light, which was not focused on quantal effects (such as entanglement) at zero temperature. In contrast, these fundamental quantum effects, which are targeted (see, e.g., [25]) in current ultracold atom research relating to fundamentals of quantum information, are central to our present paper.

Indeed, in light of the limitation of the standard Wick method [26–28] to determinantal spin-non-degenerate ground states (being restricted to the highest spin fermionic component [17,26] or to spinless bosons [20]), and thus the inability of that scheme to treat spin-degenerate ground states (ubiquitous in investigations of quantum chemistry, condensed-matter, and quantum information, e.g., the W and GHZ states studied herein), our methodology and the results we uncovered (including the highlighting and demonstration of the important role of spin resolved momentum correlations) open avenues for analysis, characterization, and understanding of recent and ongoing experiments (particularly TOF of trapped, interacting, ultracold atoms) with a focus on relevant highly entangled states as a resource in quantum information.

To put this development in context, we note here recent progress in the experimental processing of data and control and manipulation of ultracold atoms in colliding free-space beams or clouds (including free fall under the cloud's gravity) [10,11,21,23,29–31] or in optical traps and tweezers (*in situ* or TOF) [32–35], which has motivated a growing number of both experimental [10,11,21,29–35] and theoretical [12–15,36,37]

[*] constantine.yannouleas@physics.gatech.edu
[†] uzi.landman@physics.gatech.edu

studies concerning the analogies between quantum optics and matter-wave spectroscopy.

The paper is organized as follows: In Sec. II, we outline the three-site Heisenberg model and its solutions. Section III presents background material for the many-body methodology used for obtaining the momentum correlation functions, whereas Sec. IV gives results for the W states. The cases of spin unresolved momentum correlations for the W states are presented in Sec. IV A (third order) and in Sec. IV B (second order). Spin resolved momentum correlations for the W states are discussed in Sec. IV C (third order) and in Sec. IV D (second order). Results for the momentum correlation functions for the GHZ state are discussed in Sec. V. Our conclusions are given in Sec. VI.

II. OUTLINE OF THE THREE-SITE HEISENBERG MODEL AND ITS SOLUTIONS

The three-fermion $|W\rangle$ and $|\text{GHZ}\rangle$ strongly entangled three-qubit states [38,39] that are the focus of this paper are solutions [40] of the following three-site linear-spin-chain Heisenberg Hamiltonian (which describes the strong-interaction limit of the Hubbard model [41]):

$$H = (J/2)(\mathbf{S}_1 \cdot \mathbf{S}_2 + \mathbf{S}_2 \cdot \mathbf{S}_3) - J/2, \tag{1}$$

where J is the exchange coupling between sites and $\mathbf{S}_i$ is the spin operator of the particle associated with the ith site.

First we will address the case of the W states, which are the $S_z = 1/2$ eigenstates of the above Heisenberg Hamiltonian H [40].

Using the three-member ket basis $|\uparrow\uparrow\downarrow\rangle$, $|\uparrow\downarrow\uparrow\rangle$, and $|\downarrow\uparrow\uparrow\rangle$, the above Hamiltonian is written in matrix form:

$$H = \frac{J}{2}\begin{pmatrix} -1 & 1 & 0 \\ 1 & -2 & 1 \\ 0 & 1 & -1 \end{pmatrix}. \tag{2}$$

The eigenvalues of the matrix in Eq. (2) are

$$\begin{aligned} \mathcal{E}_1 &= -3J/2, \quad S = 1/2, \\ \mathcal{E}_2 &= -J/2, \quad S = 1/2, \\ \mathcal{E}_3 &= 0, \quad S = 3/2. \end{aligned} \tag{3}$$

The corresponding (normalized) eigenvectors and their total spins are given by

$$\begin{aligned} W1 &= \{1/\sqrt{6}, -\sqrt{2/3}, 1/\sqrt{6}\}^T, \quad S = 1/2, \\ W2 &= \{-1/\sqrt{2}, 0, 1/\sqrt{2}\}^T, \quad S = 1/2, \\ W3 &= \{1/\sqrt{3}, 1/\sqrt{3}, 1/\sqrt{3}\}^T, \quad S = 3/2. \end{aligned} \tag{4}$$

III. MANY-BODY METHODOLOGY FOR MOMENTUM CORRELATIONS: PRELIMINARIES

To generate the third-order momentum correlation maps $\mathcal{G}^3_i(k_1, k_2, k_3)$, with $i = 1, 2, 3$, corresponding to the three W-type solutions in Eq. (4) of the Heisenberg Hamiltonian, one needs to transition to the first-quantization formalism using momentum-dependent Wannier-type spin orbitals. To this effect, each fermionic particle in any of the three wells is represented by a displaced Gaussian function [12,13,15], which in momentum space is given by

$$\psi_j(k)\chi(\omega) = \frac{2^{1/4}\sqrt{s}}{\pi^{1/4}} e^{-k^2 s^2} e^{i d_j k}\chi(\omega). \tag{5}$$

In Eq. (5), d_j ($j = 1, 2, 3$) denotes the position of each of the three wells, and s is the width of the Gaussian function.

$\chi(\omega)$ is a shorthand notation for the spin-up, $\alpha(\omega)$, or spin-down, $\beta(\omega)$, single-particle spin functions. The two spin functions are orthonormal [42]: $\int d\omega \alpha^*(\omega)\alpha(\omega) = \int d\omega \beta^*(\omega)\beta(\omega) = 1$, $\int d\omega \alpha^*(\omega)\beta(\omega) = \int d\omega \beta^*(\omega)\alpha(\omega) = 0$.

Employing the fact that in the first-quantization representation the basis kets, $|\uparrow\uparrow\downarrow\rangle$, $|\uparrow\downarrow\uparrow\rangle$, and $|\downarrow\uparrow\uparrow\rangle$, correspond for fermions to determinants built out from the $\psi_j(k)\chi(\omega)$, with $j = 1, 2, 3$, spin orbitals, one finds that the general form of the many-body wave functions associated with the three vectors in Eq. (4) is

$$\Psi_i = \sum_{l=1}^{3} F^i_l(k_1, k_2, k_3)\zeta_l(\omega_1, \omega_2, \omega_3), \tag{6}$$

where the three spin primitives are given by $\zeta_1 = \alpha(\omega_1)\alpha(\omega_2)\beta(\omega_3)$, $\zeta_2 = \alpha(\omega_1)\beta(\omega_2)\alpha(\omega_3)$, and $\zeta_3 = \beta(\omega_1)\alpha(\omega_2)\alpha(\omega_3)$.

IV. RESULTS: THE W STATES

A. Spin unresolved third-order momentum correlations

Since the spin primitive functions ζ_l's form an orthonormal set, one gets for the spin unresolved third-order correlations [12] (i.e., summing over all possible spin cases using the formal integration over spins)

$$\begin{aligned} \mathcal{G}^3_i(k_1, k_2, k_3) &= \int \Psi^*_i \Psi_i d\omega_1 d\omega_2 d\omega_3 \\ &= \sum_{l=1}^{3} \left|F^i_l(k_1, k_2, k_3)\right|^2. \end{aligned} \tag{7}$$

The calculations of the F^i_l's out of the determinants are straightforward, but lengthy. We have used the algebraic language MATHEMATICA [43] to carry them out. Below, we present the final analytic results.

Assuming equal separations between the central and the outer wells (i.e., taking $d_1 = -D$, $d_2 = 0$, $d_3 = D$), the analytic expressions for the spin unresolved third-order momentum correlations corresponding to the three entangled $S_z = 1/2$ Heisenberg states are given by the same general formula:

$$\begin{aligned} \mathcal{G}^3_i(k_1, k_2, k_3) = {} & \frac{2\sqrt{2}}{3\pi^{3/2}} s^3 e^{-2(k_1^2+k_2^2+k_3^2)s^2} \\ & \times \Bigg\{3 + \sum_{p<q}^{3} A_i \cos[D(k_p - k_q)] \\ & + \sum_{p<q}^{3} B_i \cos[2D(k_p - k_q)] \\ & + \sum_{(p,q,r)} C_i \cos[D(k_p + k_q - 2k_r)]\Bigg\}, \end{aligned} \tag{8}$$

TABLE I. Coefficients entering in Eq. (8).

i	E_i	A_i	B_i	C_i
3	0	−2	−1	2
2	$-J/2$	−1	1	−1
1	$-3J/2$	1	−1	−1

where (p, q, r) takes only the three values (1,2,3), (2,3,1), and (3,1,2). The associated coefficients A_i, B_i, and C_i are given in Table I.

Illustrations of the unresolved third-order momentum correlations for the three W states in Eq. (4) are displayed in Fig. 1. The left column displays three-dimensional isosurface contours, $\mathcal{G}_i^3(k_1, k_2, k_3) = \text{const}$, while the right column displays corresponding two-dimensional cuts by keeping the third momentum fixed at $k_3 = 0$. The plots illustrate visually

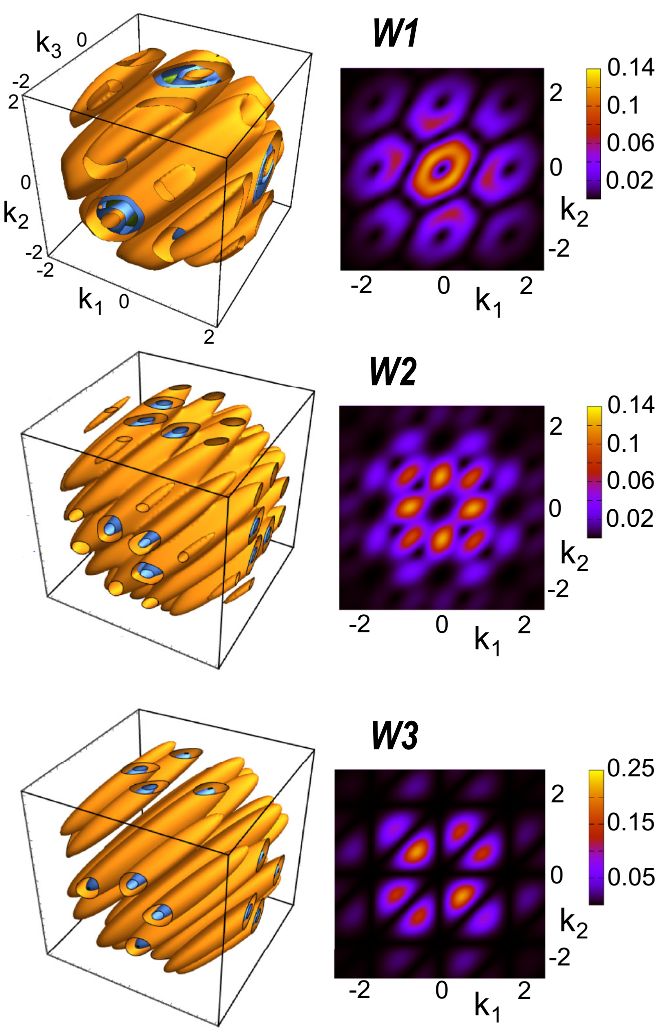

FIG. 1. Third-order spin unresolved momentum correlations [see Eq. (8)] for the three W states. Left column: 3D contour plots. Right column: Corresponding two-dimensional maps for cuts at $k_3 = 0$. Top row: $W1$. Second row: $W2$. Third row: $W3$. Parameters: $s = 0.5$ μm and $D = 3.8$ μm. Momenta in units of $1/\mu$m. Third-order correlations in units of μm^3.

that the three $\mathcal{G}_i^3(k_1, k_2, k_3)$ in Eq. (8) exhibit sufficiently different map landscapes, which could be explored with experimental measurements.

Characteristic landscape patterns that allow differentiation between the W states remain also prominent in the case of both spin unresolved and spin resolved second-order correlation maps, which are investigated next.

B. Spin unresolved second-order momentum correlations

When the N-particle many-body wave function Ψ is available in the coordinate space, it is well known that the Mth-order ($M \leqslant N$) space correlations are obtained by carrying out the $N - M$ integrations of $\Psi^*\Psi$ over the remaining $M + 1, M + 2, \ldots, N$ variables [12,44]. In this case the corresponding Mth-order momentum correlations are determined via an appropriate Fourier transform of the space correlations [12]. Here, the third-order correlations are already available in momentum space at the very beginning [see Eqs. (7) and (8)]. Thus the lower spin unresolved second-order correlations can be obtained simply from Eq. (8) by integrating $\mathcal{G}_i^3$ over the third k_3 momentum variable. Then, neglecting the vanishing contributions from the orbital overlaps (i.e., assuming $D^2/s^2 \gg 1$), one finds

$$\begin{aligned}\mathcal{G}_i^2(k_1, k_2) &= \int dk_3 \mathcal{G}_i^3(k_1, k_2, k_3)\\ &= \frac{2}{3\pi} s^2 e^{-2(k_1^2+k_2^2)s^2}\{3 + A_i \cos[D(k_1 - k_2)]\\ &\quad + B_i \cos[2D(k_1 - k_2)]\},\end{aligned} \tag{9}$$

where the coefficients A_i and B_i are the same as in Table I.

The spin unresolved second-order correlations for the three W states are plotted in the first column (for $W1$ and $W2$) and the fourth column, top row (for $W3$) of Fig. 2. It is characteristic that the main diagonal ($k_1 - k_2 = 0$) acquires nonvanishing values for the two states with $S = 1/2$, $S_z = 1/2$ (i.e., for $W1$ and $W2$), while it exhibits vanishing values all along its extent for the third ($W3$) state with $S = 3/2$, $S_z = 1/2$. Furthermore, the interference between the two length scales, D and $2D$ [see Eq. (9)], generates a wavy doubling ($W1$ and $W3$) or tripling ($W2$) of the dominant peaks of the fringes, which experimentally could be seen as broadening of the fringes. Note that this wavy broadening of the fringes was reported in [12] for the partial case of the $W1$ ground state.

C. Spin resolved third-order correlations

Spin resolved correlations impose specific values for the spins associated with the momenta variables k_i's. We note that knowledge of the spin resolved correlations provides a more complete degree of characterization of the many-body state compared to that obtained from knowledge of the spin unresolved correlations.

When the spins for all three momenta k_i's are fixed, each vector solution in Eq. (4) allows three spin arrangements according to the three spin primitives ζ_1, ζ_2, and ζ_3. As a result, the following third-order three spin resolved correlations for

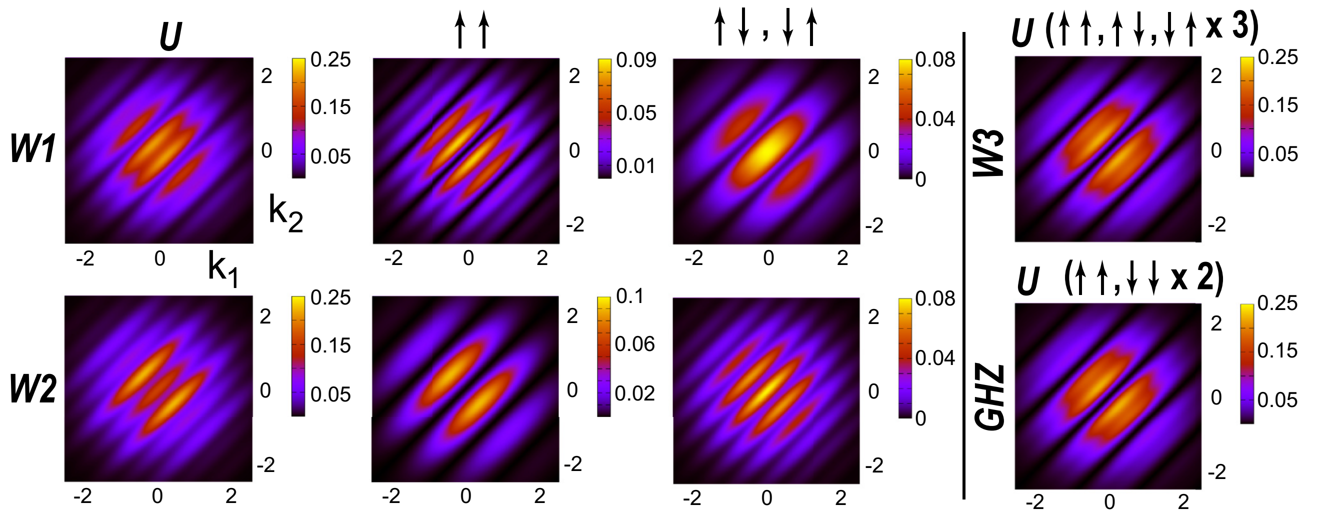

FIG. 2. Second-order momentum correlation maps for the W and GHZ states. Top row: $W1$ state and $W3$ state (fourth column). Bottom row: $W2$ state and GHZ state (fourth column). The spin unresolved correlations are denoted by a U (first and fourth column). Second and third column: Spin resolved cases denoted by the symbols ↑↑, ↑↓, and ↓↑. Other cases that coincide with the corresponding U maps when multiplied by a factor of 3 or 2 are indicated within the parentheses in the fourth column. Parameters: $s = 0.5\ \mu$m and $D = 3.8\ \mu$m. Momenta are in units of $1/\mu$m. Second-order correlations are in units of $\mu\mathrm{m}^2$.

the three Wi, with $i = 1, 2, 3$, states can be specified:

$$\mathcal{G}^{3,i}_{\uparrow\uparrow\downarrow}(k_1,k_2,k_3) = \left|F^i_1(k_1,k_2,k_3)\right|^2, \tag{10}$$

$$\mathcal{G}^{3,i}_{\uparrow\downarrow\uparrow}(k_1,k_2,k_3) = \left|F^i_2(k_1,k_2,k_3)\right|^2, \tag{11}$$

$$\mathcal{G}^{3,i}_{\downarrow\uparrow\uparrow}(k_1,k_2,k_3) = \left|F^i_3(k_1,k_2,k_3)\right|^2. \tag{12}$$

The explicit analytic expressions (a total of 9) for the above all-three-spin resolved correlations, which are different from each other, are given in a compact form by the same general expression:

$$\begin{aligned}
&\mathcal{G}^{3,i}_{\text{spin resolved}}(k_1,k_2,k_3)\\
&= \frac{\sqrt{2}}{9\pi^{3/2}} s^3 e^{-2(k_1^2+k_2^2+k_3^2)s^2}\\
&\quad \times \{6 + c_{12}\cos[D(k_1-k_2)] + c_{13}\cos[D(k_1-k_3)]\\
&\quad + c_{23}\cos[D(k_2-k_3)] + \widetilde{c}_{12}\cos[2D(k_1-k_2)]\\
&\quad + \widetilde{c}_{13}\cos[2D(k_1-k_3)] + \widetilde{c}_{23}\cos[2D(k_2-k_3)]\\
&\quad + c_{123}\cos[D(k_1+k_2-2k_3)]\\
&\quad + c_{231}\cos[D(k_2+k_3-2k_1)]\\
&\quad + c_{312}\cos[D(k_3+k_1-2k_2)]\},
\end{aligned} \tag{13}$$

where the corresponding coefficients are listed in Table II.

D. Spin resolved second-order correlations

We turn now to studying second-order spin resolved correlations. The $1\uparrow 2\uparrow$ spin resolved correlations for the three W states in Eq. (4) have the general form

$$\begin{aligned}
\mathcal{G}^{2,i}_{\uparrow\uparrow}(k_1,k_2) &= \int dk_3 \mathcal{G}^{3,i}_{\uparrow\uparrow\downarrow}(k_1,k_2,k_3) = \frac{1}{9\pi} s^2 e^{-2(k_1^2+k_2^2)s^2}\\
&\quad \times \{6 + P_i \cos[D(k_1-k_2)]\\
&\quad + Q_i \cos[2D(k_1-k_2)]\},
\end{aligned} \tag{14}$$

where the coefficients P_i and Q_i are given in Table III. Similarly, the other two second-order spin resolved correlations, namely, the $1\uparrow 2\downarrow$, $\mathcal{G}^{2,i}_{\uparrow\downarrow}(k_1,k_2) = \int dk_3 \mathcal{G}^{3,i}_{\uparrow\downarrow\uparrow}(k_1,k_2,k_3)$ correlation and the $1\downarrow 2\uparrow$, $\mathcal{G}^{2,i}_{\downarrow\uparrow}(k_1,k_2) = \int dk_3 \mathcal{G}^{3,i}_{\downarrow\uparrow\uparrow}(k_1,k_2,k_3)$ correlation, yield the same general form as in Eq. (14), with the specific values of the P_i and Q_i coefficients displayed in Table III.

The second-order spin resolved correlation maps for the two $W1$ and $W2$ states (with $S = 1/2$) are displayed in the second and third column of Fig. 2, respectively; for the $W3$ state (with $S = 3/2$), see below. The $1\uparrow 2\downarrow$ and $1\downarrow 2\uparrow$ maps for both states coincide, as indicated in the figure. The main diagonal in these maps ($k_1 - k_2 = 0$) is associated with vanishing values (resulting in fringe valleys) for the same-spin cases (↑↑), while it exhibits nonvanishing values (resulting in fringe ridges) for the different-spin cases (↑↓ or ↓↑); this is consistent with the Pauli exclusion principle for same-spin fermions and the property that fermions with different spins are distinguishable. Furthermore, there is a clear contrast regarding the number of fringes for the spin resolved maps

TABLE II. Coefficients entering in Eq. (13) for the third-order spin resolved momentum correlations.

W state	Spins	c_{12}	c_{13}	c_{23}	$\widetilde{c}_{12}$	$\widetilde{c}_{13}$	$\widetilde{c}_{23}$	c_{123}	c_{231}	c_{312}
$W3$	↑↑↓	−4	−4	−4	−2	−2	−2	4	4	4
	↑↓↑	−4	−4	−4	−2	−2	−2	4	4	4
	↓↑↑	−4	−4	−4	−2	−2	−2	4	4	4
$W2$	↑↑↓	−6	0	0	0	3	3	−6	0	0
	↑↓↑	0	−6	0	3	0	3	0	0	−6
	↓↑↑	0	0	−6	3	3	0	0	−6	0
$W1$	↑↑↓	−2	4	4	−4	−1	−1	2	−4	−4
	↑↓↑	4	−2	4	−1	−4	−1	−4	−4	2
	↓↑↑	4	4	−2	−1	−1	−4	−4	2	−4

TABLE III. Coefficients for the second-order spin resolved momentum correlations $\mathcal{G}^{2,i}_{\uparrow\uparrow}(k_1,k_2)$, $\mathcal{G}^{2,i}_{\uparrow\downarrow}(k_1,k_2)$, and $\mathcal{G}^{2,i}_{\downarrow\uparrow}(k_1,k_2)$ entering in Eq. (14). The index i counts the W states in Eq. (4).

		↑↑		↑↓		↓↑	
i	E_i	P_i	Q_i	P_i	Q_i	P_i	Q_i
3	0	−4	−2	−4	−2	−4	−2
2	$-J/2$	−6	0	0	3	0	3
1	$-3J/2$	−2	−4	4	−1	4	−1

of the $W1$ and $W2$ states; indeed for the same-spin cases (second column of Fig. 2), there are eight visible fringes for $W1$ compared to only four visible fringes for $W2$. For the different-spin cases (third column of Fig. 2), the opposite trend appears, namely, there are only five visible fringes for $W1$ compared to nine visible fringes for $W2$. Note that the sum of the three spin resolved correlations equals the spin unresolved one, symbolically $\uparrow\uparrow + \uparrow\downarrow + \downarrow\uparrow = U$.

For the $W3$ case (with $S = 3/2$, $S_z = 1/2$), all three spin resolved maps coincide. Each one of these maps multiplied by a factor of 3 equals the spin unresolved map; this is symbolically denoted at the top of the frame situated on the top row, fourth column of Fig. 2.

V. RESULTS: THE GHZ STATE

The GHZ state is a linear superposition of the two fully polarized eigenstates of the Heisenberg Hamiltonian in Eq. (1), that is,

$$|\mathrm{GHZ}\rangle = (|\uparrow\uparrow\uparrow\rangle + |\downarrow\downarrow\downarrow\rangle)/\sqrt{2}. \tag{15}$$

The corresponding energy is $E_{\mathrm{GHZ}} = 0$ and the total spins are $S = 3/2$ (a spin eigenvalue) and $\langle S_z\rangle = 0$ (an expectation value, not a spin eigenvalue). The second-order spin unresolved correlation map for the GHZ state is displayed in Fig. 2 (second row, fourth column). It is immediately seen that the GHZ spin unresolved map coincides with that of the $W3$ spin unresolved map displayed also in Fig. 2, top of fourth column. This result was also explicitly verified by deriving via our methodology the corresponding analytic GHZ expression and comparing it with that in Eq. (9) (for $i = 3$). Namely, starting from the associated determinants for the two $|\uparrow\uparrow\uparrow\rangle$ and $|\downarrow\downarrow\downarrow\rangle$ kets in Eq. (15), we first calculated the third-order GHZ momentum correlations and we subsequently derived the second-order correlations through an integration over the third momentum k_3 variable. Furthermore, the GHZ second-order spin resolved correlation maps, ↑↑ and ↓↓, coincide and equal the spin unresolved one when multiplied by a factor of 2. Finally and consistent with the above, we found through our analytic calculations (not shown) that the GHZ third-order spin unresolved correlation maps coincide with those associated separately with each fully polarized state $|\uparrow\uparrow\uparrow\rangle$ ($S = 3/2$, $S_z = 3/2$) or $|\downarrow\downarrow\downarrow\rangle$ ($S = 3/2$, $S_z = -3/2$), as well as with that of the $W3$ state (which also has $S = 3/2$) [see Eq. (8), for $i = 3$].

VI. CONCLUSIONS

Analytical expressions for the third-order and second-order spin resolved and spin unresolved momentum correlations for the strongly entangled W and GHZ states [38,39] of three singly trapped ultracold fermionic atoms have been derived. The associated correlation patterns and maps are related [15] to current experimentally accessible TOF measurements; they enable matter-wave interference studies in analogy with recent three-photon interferometry [45–48]. A main finding is that knowledge of the spin unresolved correlation maps is required to fully characterize the strongly entangled states.

This paper uncovers and demonstrates a methodology which allows treatment of strongly interacting entangled states which are outside the scope of the standard Wick factorization scheme [17,20,21], thus opening the door and providing the impetus for experimental investigations, using coincidence time-of-flight measurements on trapped ultracold atom systems, of entangled states (like the W and GHZ ones treated here) which are ubiquitous in quantum information theory and protocols in quantum communication and cryptography and studies of the fundamentals of quantum mechanics [49].

Note added. Recently, an experimental study appeared (see [16]), where the results of time-of-flight measurements of second-order position and momentum correlations for entangled Einstein-Podolsky-Rosen states of two ultracold fermionic atoms have been presented. A second experimental study has also appeared (see [17]), where Wick's theorem is utilized for analysis of time-of-flight measurements of a noninteracting spin-polarized state (unentangled, single determinant, highest spin component) of optical-tweezer-trapped three ^{6}Li ultracold atoms.

ACKNOWLEDGMENTS

This work has been supported by the Air Force Office of Scientific Research under Grant No. FA9550-15-1-0519. Calculations were carried out at the Georgia Institute of Technology Center for Computational Materials Science.

[1] R. J. Glauber, The quantum theory of optical coherence, Phys. Rev. **130**, 2529 (1963).
[2] R. J. Glauber, Nobel Lecture: One hundred years of light quanta, Rev. Mod. Phys. **78**, 1267 (2006).
[3] R. Hanbury Brown and R. Q. Twiss, Correlation between photons in two coherent beams of light, Nature (London) **177**, 27 (1956).
[4] L. Mandel, Quantum effects in one-photon and two-photon interference, Rev. Mod. Phys. **71**, S274 (1999).
[5] Y. H. Shih, *An Introduction to Quantum Optics: Photon and Biphoton Physics* (CRC, Boca Raton, FL, 2011).
[6] Z. Y. Ou, *Multi-Photon Quantum Interference* (Springer, New York, 2007).

[7] C. K. Hong, Z. Y. Ou, and L. Mandel, Measurement of Subpicosecond Time Intervals between Two Photons by Interference, Phys. Rev. Lett. **59**, 2044 (1987).

[8] J. Schwinger, On the Green's functions of quantized fields. I., Proc. Natl Acad. Sci. USA **37**, 452 (1951).

[9] J. Schwinger, On the Green's functions of quantized fields. II., Proc. Natl Acad. Sci. USA **37**, 455 (1951).

[10] S. S. Hodgman, R. I. Khakimov, R. J. Lewis-Swan, A. G. Truscott, and K. V. Kheruntsyan, Solving the Quantum Many-Body Problem via Correlations Measured with a Momentum Microscope, Phys. Rev. Lett. **118**, 240402 (2017).

[11] Th. Schweigler, V. Kasper, S. Erne, I. Mazets, B. Rauer, F. Cataldini, T. Langen, Th. Gasenzer, J. Berges, and J. Schmiedmayer, Experimental characterization of a quantum many-body system via higher-order correlations, Nature (London) **545**, 323 (2017).

[12] B. B. Brandt, C. Yannouleas, and U. Landman, Two-point momentum correlations of few ultracold quasi-one-dimensional trapped fermions: Diffraction patterns, Phys. Rev. A **96**, 053632 (2017).

[13] B. B. Brandt, C. Yannouleas, and U. Landman, Interatomic interaction effects on second-order momentum correlations and Hong-Ou-Mandel interference of double-well-trapped ultracold fermionic atoms, Phys. Rev. A **97**, 053601 (2018)

[14] C. Yannouleas and U. Landman, Anyon optics with time-of-flight two-particle interference of double-well-trapped interacting ultracold atoms, Phys. Rev. A **100**, 013605 (2019).

[15] C. Yannouleas, B. B. Brandt, and U. Landman, Interference, spectral momentum correlations, entanglement, and Bell inequality for a trapped interacting ultracold atomic dimer: Analogies with biphoton interferometry, Phys. Rev. A **99**, 013616 (2019).

[16] A. Bergschneider, V. M. Klinkhamer, J. H. Becher, R. Klemt, L. Palm, G. Zürn, S. Jochim, and Ph. M. Preiss, Experimental characterization of two-particle entanglement through position and momentum correlations, Nat. Phys. **15**, 640 (2019).

[17] Ph. M. Preiss, J. H. Becher, R. Klemt, V. Klinkhamer, A. Bergschneider, and S. Jochim, High-Contrast Interference of Ultracold Fermions, Phys. Rev. Lett. **122**, 143602 (2019).

[18] G. C. Wick, The evaluation of the collision matrix, Phys. Rev. **80**, 268 (1950).

[19] J. Zinn-Justin, *Quantum Field Theory and Critical Phenomena* (Oxford University, New York, 2002).

[20] C. Carcy, H. Cayla, A. Tenart, A. Aspect, M. Mancini, and D. Clément, Momentum-space atom correlations in a Mott insulator, arXiv:1904.10995.

[21] S. S. Hodgman, R. G. Dall, A. G. Manning, K. G. H. Baldwin, and A. G. Truscott, Direct measurement of long-range third-order coherence in Bose-Einstein condensates, Science **331**, 1046 (2011).

[22] See the Supporting Online Material of [21].

[23] A. G. Manning, Wu RuGway, S. S. Hodgman, R. G. Dall, K. G. H. Baldwin, and A. G. Truscott, Third-order spatial correlations for ultracold atoms, New J. Phys. **15**, 013042 (2013).

[24] J. V. Gomes, A. Perrin, M. Schellekens, D. Boiron, C. I. Westbrook, and M. Belsley, Theory for a Hanbury Brown Twiss experiment with a ballistically expanding cloud of cold atoms, Phys. Rev. A **74**, 053607 (2006).

[25] R. Islam, R. Ma, Ph. M. Preiss, M. E. Tai, A. Lukin, M. Rispoli, and M. Greiner, Measuring entanglement entropy in a quantum many-body system, Nature (London) **528**, 77 (2015).

[26] L. S. Cederbaum and J. Schirmer, Green's functions for open-shell atoms and molecules, Z. Phys. **271**, 221 (1974).

[27] M. Wagner, Expansions of nonequilibrium Green's functions, Phys. Rev. B **44**, 6104 (1991).

[28] R. van Leeuwen and G. Stefanucci, Wick theorem for general initial states, Phys. Rev. B **85**, 115119 (2012).

[29] T. Jeltes, J. M. McNamara, W. Hogervorst, W. Vassen, V. Krachmalnicoff, M. Schellekens, A. Perrin, H. Chang, D. Boiron, A. Aspect, and C. I. Westbrook, Comparison of the Hanbury Brown–Twiss effect for bosons and fermions, Nature (London) **445**, 402 (2007).

[30] R. G. Dall, A. G. Manning, S. S. Hodgman, Wu RuGway, K. V. Kheruntsyan, and A. G. Truscott, Ideal n-body correlations with massive particles, Nat. Phys. **9**, 341 (2013).

[31] R. Lopes, A. Imanaliev, A. Aspect, M. Cheneau, D. Boiron, and C. I. Westbrook, Atomic Hong-Ou-Mandel experiment, Nature (London) **520**, 66 (2015).

[32] S. Fölling, F. Gerbier, A. Widera, O. Mandel, T. Gericke, and I. Bloch, Spatial quantum noise interferometry in expanding ultracold atom clouds, Nature (London) **434**, 491 (2005).

[33] A. M. Kaufman, B. J. Lester, C. M. Reynolds, M. L. Wall, M. Foss-Feig, K. R. A. Hazzard, A. M. Rey, and C. A. Regal, Two-particle quantum interference in tunnel-coupled optical tweezers, Science **345**, 306 (2014).

[34] S. Murmann, A. Bergschneider, V. M. Klinkhamer, G. Zürn, T. Lompe, and S. Jochim, Two Fermions in a Double Well: Exploring a Fundamental Building Block of the Hubbard Model, Phys. Rev. Lett. **114**, 080402 (2015).

[35] A. M. Kaufman, M. C. Tichy, F. Mintert, A. M. Rey, and C. A. Regal, The Hong-Ou-Mandel effect with atoms, Adv. Atom. Mol. Opt. Phys. **67**, 377 (2018).

[36] R. J. Lewis-Swan and K. V. Kheruntsyan, Proposal for demonstrating the Hong-Ou-Mandel effect with matter waves, Nat. Commun. **5**, 3752 (2014).

[37] M. Bonneau, W. J. Munro, K. Nemoto, and Jörg Schmiedmayer, Characterizing twin-particle entanglement in double-well potentials, Phys. Rev. A **98**, 033608 (2018).

[38] D. M. Greenberger, M. A. Horne, A. Shimony, and A. Zeilinger, Bell's theorem without inequalities, Am. J. Phys. **58**, 1131 (1990).

[39] W. Dür, G. Vidal, and J. I. Cirac, Three qubits can be entangled in two inequivalent ways, Phys. Rev. A **62**, 062314 (2000).

[40] A. K. Rajagopal and R. W. Rendell, Robust and fragile entanglement of three qubits: Relation to permutation symmetry, Phys. Rev. A **65**, 032328 (2002).

[41] A. Auerbach, *Interacting Electrons and Quantum Magnetism* (Springer-Verlag, New York, 1994).

[42] A. Szabo and N. S. Ostlund, *Modern Quantum Chemistry: Introduction to Advanced Electronic Structure Theory*, revised 1st ed. (McGraw-Hill, New York, 1989), see in particular pp. 45 and 52.

[43] MATHEMATICA, version 11.3, Wolfram Research, Champaign, IL, 2018.

[44] P.-O. Löwdin, Quantum theory of many-particle systems. I. Physical interpretations by means of density matrices, natural

spin-orbitals, and convergence problems in the method of configurational interaction, Phys. Rev. **97**, 1474 (1955).

[45] S. Agne, Th. Kauten, J. Jin, E. Meyer-Scott, J. Z. Salvail, D. R. Hamel, K. J. Resch, G. Weihs, and Th. Jennewein, Observation of Genuine Three-Photon Interference, Phys. Rev. Lett. **118**, 153602 (2017).

[46] A. J. Menssen, A. E. Jones, B. J. Metcalf, C. Tichy, S. Barz, W. S. Kolthammer, and I. A. Walmsley, Distinguishability and Many-Particle Interference, Phys. Rev. Lett. **118**, 153603 (2017).

[47] V. Tamma and S. Laibacher, Multiboson Correlation Interferometry with Arbitrary Single-Photon Pure States, Phys. Rev. Lett. **114**, 243601 (2015).

[48] S. Laibacher and V. Tamma, Symmetries and entanglement features of inner-mode-resolved correlations of interfering nonidentical photons, Phys. Rev. A **98**, 053829 (2018).

[49] D. M. Greenberger, M. A. Horne, and A. Zeilinger, Going beyond Bell's theorem, in *Bell's Theorem, Quantum Theory, and Conceptions of the Universe*, edited by M. Kafatos (Kluwer, Dordrecht, 1989), pp. 69–72.